Supporting Information of

Not All Types of Secondary Organic Aerosol Mix: Two Phases Observed When Mixing Different Secondary Organic Aerosol Types

Fabian Mahrt[1,2], Long Peng[1,3], Julia Zaks[1], Yuanzhou Huang[1,†], Paul E. Ohno[4,5], Natalie R. Smith[6], Florence K.A. Gregson[1], Yiming Qin[4,§], Celia L. Faiola[6], Scot T. Martin[4,7], Sergey A. Nizkorodov[6], Markus Ammann[2] and Allan K. Bertram[1,*]

[1]Department of Chemistry, University of British Columbia, 2036 Main Mall, Vancouver, BC, V6T1Z1 Canada
[2]Laboratory of Environmental Chemistry, Paul Scherrer Institute, 5232 Villigen, Switzerland
[3]Institute for Environmental and Climate Research, Jinan University, Guangzhou 511443, China
[4]John A. Paulson School of Engineering and Applied Sciences, Harvard University, Cambridge, MA 02138, USA
[5]Center for the Environment, Harvard University, Cambridge, MA 02138, USA
[6]Department of Chemistry, University of California, Irvine, Irvine, CA 92697, USA.
[7]Department of Earth and Planetary Sciences, Harvard University, Cambridge, MA 02138, USA
[†]Now at: Anton Paar Canada Inc., 4920 Place Olivia, H4R 2Z8 Saint Laurent, Canada
[§]Now at: Department of Chemistry, University of California, Irvine, CA 92697-2025, USA

Correspondence to: Allan K. Bertram (bertram@chem.ubc.ca)

This file includes:

S1 Summary of previous studies

1.1 Overview of results from previous studies that mixed one SOA type generated in environmental reactors with a commercial, single-component SOA proxy

Table S1: Summary of previous studies that investigated the miscibility of SOA mixtures, where a SOA material was produced in an environmental reactor from ozonolysis of α-pinene and mixed with a commercial, single-component SOA proxy. Indicated are the SOA types, the relative humidity (RH) at which the experiment was performed, and whether mixing was reported or not. The O/C ratio listed for the α-pinene SOA material is based on Canagaratna et al. (2015). N/A indicates not available.

SOA_1 (O/C)	SOA_2 (O/C) (Proxy)	RH value or range	Mixing observed	Extent of mixing observed	Reference
α-pinene ozonolysis (0.41)	Glycerol (1.0)	12%	Yes	1-phase particles[γ]	Gorkowski et al. (2020)
α-pinene ozonolysis (0.41)	Glycerol (1.0)	73%	No	2-phase particles[γ]	Gorkowski et al. (2017)
α-pinene ozonolysis (0.41)	Erythritol (1.0)	55% to 65%	No[*]	N/A	Gordon et al. (2016)
α-pinene ozonolysis (0.41)	Tetraethylene glycol (0.625)	55% to 65%	Yes[*,a]	N/A	Gordon et al. (2016)
α-pinene ozonolysis (0.41)	Adipic acid (0.66)	2%	No[$]	N/A	Song et al. (2011)
α-pinene ozonolysis (0.41)	Fulvic acid (0.76)[b]	2%	No[$]	N/A	Song et al. (2011)
α-pinene ozonolysis (0.41)	Citric acid (1.16)	2%	Yes[$]	N/A	Song et al. (2011)
α-pinene ozonolysis (0.41)	Adipic acid (0.66)	60%	No[$]	N/A	Song et al. (2011)
α-pinene ozonolysis (0.41)	Fulvic acid (0.76)[b]	60%	No[$]	N/A	Song et al. (2011)
α-pinene ozonolysis (0.41)	Citric acid (1.16)	60%	Yes[$,c]	N/A	Song et al. (2011)
α-pinene ozonolysis (0.41)	Tetraethylene glycol (0.625)	< 20%	Yes[*]	N/A	Ye et al. (2016a)
α-pinene ozonolysis (0.41)	Levoglucosan (0.83)	< 20%	No[*]	N/A	Ye et al. (2016a)
α-pinene ozonolysis (0.41)	Erythriol (1.0)	< 20%	No[*]	N/A	Ye et al. (2016a)
α-pinene ozonolysis (0.41)	Citric acid (1.16)	< 20%	Yes[*]	N/A	Ye et al. (2016a)
α-pinene ozonolysis (0.41)	Tetraethylene glycol (0.625)	55% to 60%	Yes[*]	N/A	Ye et al. (2016a)
α-pinene ozonolysis (0.41)	Erythriol (1.0)	55% to 60%	No[*]	N/A	Ye et al. (2016a)
α-pinene ozonolysis (0.41)	Levoglucosan (0.83)	2% to 5%	No[$]	N/A	Ye et al. (2016a)
α-pinene ozonolysis (0.41)	Erythriol (1.0)	2% to 5%	No[$]	N/A	Ye et al. (2016a)

[*]flow tube experiment; [$]chamber experiment; [γ]aerosol optical tweezer; [a] Mixing (mass enhancement) was only found for tetraethylene glycol concentrations ≥ 80 μg m^{-3}; [b]Based on Rice and MacCarthy (1991); [c] Mixing (mass enhancement) was only found for α-pinene concentrations ≥ 95 μg m^{-3}

1.2 Overview of results from previous studies that mixed two SOA types generated in environmental reactors

Table S2: Summary of previous studies that investigated the miscibility of SOA mixtures, where both SOA types were produced in environmental reactors. Indicated are the SOA types, the relative humidity (RH) at which the experiment was performed, and whether mixing was reported or not. N/A indicates not available.

SOA_1 (O/C)	**SOA_2 (O/C)**	**RH value or range**	**Mixing observed**	**Onset and/or extent of mixing observed**	**Reference**
Toluene-D_8/OH (0.85)[#]	α-pinene/O_3 (0.41)[#]	< 5%	Yes[$]	N/A	Robinson et al. (2013)
Toluene/OH (0.85)[#]	α-pinene/O_3 (0.41)[#]	17% to 32%	Yes[$]	N/A	Hildebrandt et al. (2011)
Isoprene/OH (photooxidation products, 0.85)[#]	α-pinene/OH (0.41)[#]	50%	Yes[$]	N/A	Dommen et al. (2009)
Toluene-D_8/OH (0.6)	α-pinene /O_3; prepared in excess O_3; (0.41)[#]	~7% to ~85%	Yes[$]	Mixing observed for RH > 20%	Ye et al. (2016b)
Isoprene/O_3 (0.55)	Tolune-D_8 /OH (0.48)	~10%	Yes[$]	28%±2% (RH < 10%)	Ye et al. (2018b)
Limonene/O_3 (0.43)	α-pinene-D_6/D_3/O_3 (0.30)	~10% to 30%	Yes[$]	~15% (RH < 10%) ~20% RH > 30%)	Ye et al. (2018b)
Limonene/O_3 (0.43)	Tolune-D_8/OH (0.45)	~10% to ~30%	Yes[$]	25%±2% (RH < 10%) 30%±1% (RH > 30%)	Ye et al. (2018b)
β-caryophyllene/O_3 (0.29)	α-pinene-D_6/O_3 (0.30)	~10% to ~75%	Yes[$]	~5% (RH < 10%) ~10% (RH > 30%)	Ye et al. (2018b)
β-caryophyllene/O_3 (0.31)	Tolune-D_8/OH (0.48)	~10% to ~50%	Yes[$]	~5% (RH < 10%) ~10% (RH > 30%)	Ye et al. (2018b)

[#]Based on Canagaratna et al. (2015)(Canagaratna et al., 2015); [*]flow tube experiment; [$]chamber experiment

S2 Method of generating internal SOA+SOA mixtures

S2.1 Experimental setups and conditions used to generate SOA types in consecutive generation and impaction experiments.

The majority (12 out of 15) of the SOA+SOA mixtures studied here was prepared using the consecutive generation and impaction method. After generation of a given SOA type in one of the reactors, and prior to impaction of another SOA type on top of the hydrophobic glass slides, the SOA samples were stored in air-sealed containers in a freezer at -20 °C, to minimize evaporative loss and potential condensed phase reactions of the SOA material. Most SOA containing glass slides were used within ~3 weeks of sample storage. Using the mixture of catechol SOA deposited on top of β-caryophyllene, we verified that the phase behavior was similar between freshly deposited β-caryophyllene SOA and slides of β-caryophyllene SOA that had been frozen for 3 weeks.

For consecutive generation and impaction experiments different types of reactors have been used to generate the different SOA types, namely the University of British Columbia environmental chamber (UBC-EC), the University of British Columbia oxidation flow reactor (UBC-OFR) and the Harvard University oxidation flow reactor (HU-OFR). An overview of the reactors and the experimental conditions used to generate each of the SOA types is given in Table S3. Details for each reactor are described below.

Table S3. Overview of the reactor types, particle mass concentration and average elemental oxygen-to-carbon (O/C) and hydrogen-to-carbon (H/C) ratio of the individual SOA types studied here and used to generate internally mixed SOA+SOA particles using the consecutive generation and impaction method. Each combination of two SOA types was studied. See Table 1 of main text for the number of phases observed for each mixture. For the O/C and the H/C ratios the average value is given along with the uncertainty (12% and 4% relative error for O/C and H/C ratios), associated with the improved ambient method applied to a multi-species organic mixture (≥ 25 species), used for AMS data analysis (Canagaratna et al., 2015). Also indicated in parenthesis is the range over which the average O/C and H/C ratios varied on a day-to-day basis. MOSSI denotes multi-orifice single stage impactor and SKC denotes Sioutas cascade (slit) impactor.

SOA type	Reactor	Mass concentration / µg m^{-3}	Collection time and method	O/C	H/C
Valencene/O_3	UBC-OFR	60–120	22–26 h MOSSI or SKC	0.34 ± 0.04 (0.31 to 0.38)	1.53 ± 0.06 (1.43 to 1.57)
β-caryophyllene/O_3	UBC-EC	33–55	22–26 h MOSSI or SKC	0.40 ± 0.05 (0.32 to 0.47)	1.55 ± 0.06 (1.46 to 1.63)
Farnesene/O_3	UBC-OFR	60–100	22–26 h MOSSI or SKC	0.41 ± 0.05 (0.38 to 0.45)	1.53 ± 0.06 (1.48 to 1.6)
α-pinene/O_3	UBC-EC	22–37	22–26 h MOSSI or SKC	0.50 ± 0.06 (0.47 to 0.53)	1.62 ± 0.06 (1.57 to 1.66)
Catechol/O_3	UBC-EC	18–70	22–26 h MOSSI or SKC	0.88 ± 0.11 (0.81 to 0.94)	1.21 ± 0.05 (1.14 to 1.28)
Toluene/OH	HU-OFR	20–40	22–26 h MOSSI or SKC	1.05$^{\gamma}$ ± 0.13 (0.73 to 1.29)	1.44$^{\gamma}$ ± 0.09 (1.35 to 1.69)

$^{\gamma}$ Values based on sampling washed-off and re-aerosolized SOA particles from aqueous solution; Section S5.

UBC-EC: The environmental chamber at UBC is a 1.8 m^3 continuous flow chamber that has been described in detail previously (Maclean et al., 2021; Huang et al., 2021), and that is similar to other continuous flow environmental chambers (King et al., 2009; Shilling et al., 2008; Zhang et al., 2018). Within the environmental chamber, SOA was generated by dark ozonolysis of α-pinene (Sigma Aldrich, 98% purity), β-caryophyllene (Sigma Aldrich, ≥ 98% purity) or catechol (Sigma Aldrich, ≥ 99% purity). For all experiments ozone (O_3) was generated outside the chamber by flowing a dry (RH ≤ 1.5%), particle- and hydrocarbon-free air stream (1.75 L min^{-1}) from a zero-air generator (Aadco, model: 737) over a pen-ray style UV-lamp (λ_{mode} = 253.7 nm; Jelight, model: 610). Mixtures of 2 wt% of each volatile organic compound (VOC) in 2-butanol (Sigma-Aldrich, ≥ 99% purity) were prepared, separately for each SOA precursor. The 2-butanol serves as a scavenger for hydroxyl radicals (OH), which can be formed as a by-product in alkene-ozone reactions (Kroll et al., 2002; Paulson et al., 1999). We used a scavenger in all our experiments where SOA was produced from oxidation by O_3 to minimizing the impact of reactions of the SOA precursor with OH radicals, allowing us to largely isolate SOA formation from ozonolysis. Previous studies have shown that the reaction of the scavenger with the OH radicals does not contribute to SOA formation, while it can impact the ability of the gaseous SOA precursor to form SOA, i.e., the aerosol mass yield (Docherty and Ziemann, 2003; Keywood et al., 2004). A syringe pump (Pump: Cole-Palmer, model: 100, Syringe: Hamilton,

100-Series Gastight) was used to feed the solution of 2-butanol and the VOC into a gently heated (~318 K), round-bottom glass flask, where the organic liquid was vaporized, and carried into the environmental chamber by continuously flushing the glass flask with zero air using a flow rate of 17.5 L min^{-1}. All flows were held constant throughout an experiment, and controlled by mass flow controllers (MFC, Omega, model: FMA5400/550 A Series), resulting in an average residence time for the gases and particles of approximately 1.6 h within the environmental chamber. Syringe pump injection rates of 30 µl h^{-1} for each VOC and 2-butanol solution were used. This resulted in SOA mass loadings within the environmental chamber between approximately 18 to 100 µg m^{-3}, measured with an optical particle counter (OPC, Grimm, model: 11-S; optical flow rate: 1.2 L min^{-1}, size range 0.25–32 µm), that was used to periodically sampling air from the chamber throughout an experiment (TableS3). Ozone concentrations were continuously measured at the exit of the chamber using an O_3 monitor (ThermoScientific, model: 49i), with O_3 being in excess by approximately 300–380 ppb_v for all UBC-EC experiments using the consecutive generation and impaction method.

At the exit of the environmental chamber, the SOA particles were collected onto plain glass slides (12 mm diameter, Hampton Research, HR3-209T and ORSAtec GmbH, customized order) that were made hydrophobic through coating with either fluoropel-800 (Cytonix) or with Trichloro(1H,1H,2H,2H-perfluorooctyl)silane (Sigma Aldrich, 97% purity), to achieve a high contact angle between the glass substrate and the SOA particles. To collect SOA material for phase behavior analysis, chamber air was continuously sampled (10–12 L min^{-1}) over a period of approximately 22 h to 26 h, using either a multi-orifice single stage impactor with a 50% cut-off diameter of ~0.18 µm (MOSSI, MSP Corporation), or a slit impactor with a 50% cut-off diameter of ~0.25 µm (SKC, Sioutas Cascade Impactor).

UBC-OFR: Also used for sample generation was a 22 L volume oxidation flow reactor available at UBC to generate SOA material from ozonolysis of farnesene (Sigma Aldrich, mixture of isomers) and valencene (Sigma Aldrich, ≥ 65% purity). As in the case of the UBC-EC, O_3 was generated outside the UBC-OFR by passing a constant flow (2.0 L min^{-1}; MFC: Omega, model: FMA5400/550 A Series) of zero air over a pen-ray style UV-lamp (Jelight, model: 610) and adding it into the OFR. The output oxidant concentration of the O_3 generator can be varied by adjusting the flow rate and the sleeve length over the UV-lamp. Here the flow rate was kept constant in all our experiments and the sleeve length was adjusted to achieve O_3 concentrations of approximately 2300 ppb and 6500 ppb for the generation of farnesene and valencene SOA material, respectively, as periodically measured with an O_3 detector (2B Technologies, model: 202) at the exit (after the reaction) of the UBC-OFR. The VOC solutions (2 wt%) were prepared in 2-butanol and added to a gently heated (~318 K) glass bulb, using a syringe pump (Pump: Chemxy Inc., model: Fusion 101, Syringe: Hamilton, 1000-Series Gastight) with injection rates of 20 µl hr^{-1} for both the farnesene and valencene solutions. Within the heated glass bulb, the organic solutions were vaporized, and carried into the chamber by flushing the glass bulb with zero air. Flow rates of 3 L min^{-1} and 2 L min^{-1} were used in the case of farnesene and valencene, respectively, as controlled by a MFC (MKS, Legacy-Series). The total flow rates through the UBC-OFR were 5 L min^{-1} and 4 L min^{-1}, resulting in residence times in the OFR of around 260 s and 330 s for the farnesene and valencene experiments, respectively. Lower flow rates through the OFR in the case of valencene as compared to farnesene oxidation were used due to its slower reaction with O_3(Kim et al., 2011; Yee et al., 2018), to allow for sufficient SOA generation during the residence time. The SOA particle mass concentrations within the OFR were measured with an OPC, and typically ranged between approximately 60 µg m^{-3} to 100 µg m^{-3} (farnesene SOA) and approximately 80 µg m^{-3} to 100 µg m^{-3} (valencene SOA) for our experimental conditions (Table S3). At the exit of the UBC-OFR, the particles were collecting onto hydrophobic glass slides using either a multi-orifice single stage or a slit impactor, identical to the case of the EC-UBC sampling (see above), operated at a flow rate of ~10 L min^{-1}. Since the flow rates needed for the impactor was larger than the total flow rate from the outlet of the OFR-UBC (4–5 L min^{-1}), the air flow at the outlet of the OFR containing the SOA particles was sheathed with filtered (Pall Corporation, HEPA) particle-free, ambient air prior to collection with the impactor. Typical SOA material collection times were approximately 22 h to 26 h.

HU-OFR: Toluene derived SOA material was produced by photooxidation of toluene vapors in an OFR at Harvard University. The HU-OFR has been described in detail elsewhere(Liu et al., 2015). In brief, OH radicals were produced within the HU-OFR by photodissociation of O_3, followed by the reaction of the resulting excited atomic oxygen with water vapor. The O_3 concentration within the OFR was around ~20 ppm_v and the RH was 40% for our experiments. The toluene (Sigma Aldrich, ≥ 99.5% purity) was injected into a glass flask held at room temperature (~293 K) using a syringe pump (Chemyx Inc., model: Fusion 200), and from there flushed into the HU-OFR. The resulting SOA mass loadings in the OFR were typically between 20 µg m^{-3} to 40 µg m^{-3}, as determined from the size distribution measured with a scanning mobility particle sizer (SMPS, TSI Inc., differential mobility analyzer model 3081, condensation particle counter model 3010, aerosol-to-sheath flow ratio: 5:1, particle electric mobility diameter range: 10–530 nm) and assuming ρ = 1200 kg m^{-3} for the material density (Shilling et al., 2008). The total volumetric flow rate through the HU-OFR was 7 L min^{-1}, resulting in a particle residence time of 110 s(Liu et al., 2015). Toluene SOA material was collected onto hydrophobic glass slides using a custom-built single-

stage impactor (Song et al., 2017), by continuously sampling air from the HU-OFR at a flow rate of 3 L min^{-1}, over a period of approximately 22 h to 26 h.

S2.2 Experimental setup and conditions used to generate SOA in simultaneous generation and impaction experiments.

A handful (3 out of 15) of the SOA+SOA mixtures studied here were prepared in the UBC-EC, using the simultaneous generation and impaction method. Specifically, the simultaneous generation and impaction method was used for mixtures of α-pinene/O_3+catechol/O_3, β-caryophyllene/O_3+catechol/O_3 and α-pinene/O_3+β-caryophyllene/O_3 (Table 1). For these experiments two different SOA precursors were simultaneously added to and simultaneously oxidized by ozonolysis within the UBC-EC. Overall, the experimental setup and instrumentation used was similar to that described in Section S2.1 when the UBC-EC was used to generate SOA material from a single VOC. In order to add and oxidize two different VOC types simultaneously to the UBC-EC two independent sets of a syringe pumps and a heated (~318 K) glass flask were used. Each syringe pump (Pump: Cole-Palmer, model: 100 or Pump: Cole-Palmer, model: Masterflex 78-0100C) was used to add a 2 wt% VOC solution in 2-butanol into a heated glass flask. The two heated glass flasks were coupled in series upstream of the UBC-EC. Thus, the VOC vapors from the first flask were flushed through the second flask, and from there the combined organic vapors were carried into the environmental chamber, using dry (< 1.5% RH) air from a zero-air generator (Aadco, model: 737) and a flow rate of 17.5 L min^{-1}, controlled by a mass flow controller, as described in Section S1. Syringe pump injection rates of 30 µl h^{-1} for each VOC and 2-butanol solution were used for all simultaneous generation and impaction experiments. Ozone was added to the UBC-EC in an identical fashion as for the consecutive impaction and generation experiments, using a pen-style UV lamp (Jelight, model: 610), flushed with zero-air at a rate of 1.75 L min^{-1}. The O_3 concentration was continuously measured at the exit of the UBC-EC using an O_3 monitor (ThermoScientific, model: 49i), with O_3 being in excess by approximately 250–300 ppb_v for all experiments when two VOCs were added to the UBC-EC. The SOA mass loadings within the UBC-EC for the simultaneous generation and impaction experiments were around 90 µg m^{-3}, as measured with an OPC (Grimm, model: 11-S).

To estimate the individual contribution of each individual SOA type to the total organic particle mass concentrations when both SOA types were present within the UBC-EC, the simultaneous generation and impaction experiments were carried out as follows, and as schematically depicted in Fig. S1: At the beginning of each experiment, only one VOC was injected into the UBC-EC, until the organic mass concentration reached a steady state, as monitored with the OPC. After a steady state had been reached, the injection of the second VOC was started at time t_1, causing an overall increase in total aerosol mass within the chamber, resulting from the additional oxidation and SOA formation of the second VOC. After some time t_2 the overall organic mass concentration approached a new steady state, with contributions of both VOCs becoming simultaneously oxidized and forming SOA particles. Only samples collected during this period, i.e., when both SOA types were simultaneously injected and oxidized, and a steady-state mass loading had been reached, were used for phase behavior analysis of SOA+SOA mixtures generated by the simultaneous generation and impaction method. Lastly, the injection of the first VOC was stopped at time t_3, and the total mass loading decreased to a new steady state after time t_4. The average organic mass concentrations when only either one of the SOA types was present within the chamber were then used to estimate the contributions of the two SOA types to the total mass of a SOA+SOA mixtures and to estimate a SOA-to-SOA mass mixing ratio (see below). The average total organic mass concentrations along with the mass concentrations of the individual SOA types before and after each simultaneous generation and impaction experiment are summarized in Table S4.

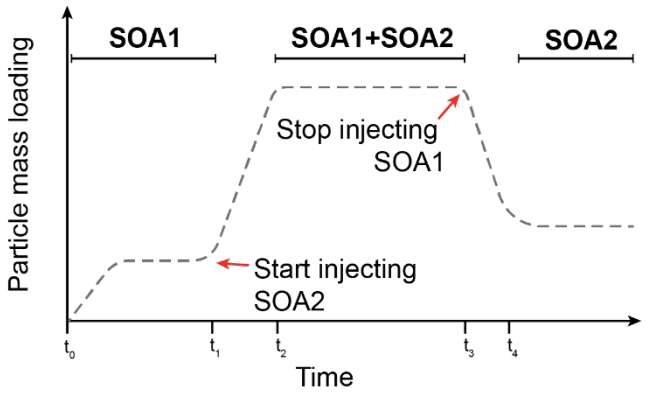

Figure S1: Schematic illustration of the temporal evolution of particle mass loading during experiments when two SOA types were simultaneously generated in the UBC-EC and simultaneously impacted to produce SOA+SOA particles.

Table S4. Overview of the SOA+SOA mixtures prepared using the simultaneous generation and impaction method along with particle mass loadings. For these experiments the UBC-EC was used. We assume the average elemental O/C and H/C ratios of the different SOA types to be the same as in the experiments using the consecutive generation and impaction method when one SOA type was present within the UBC-EC (Table S3). The values in parenthesis indicate the standard error of the mass loading, given as two standard deviations.

Exp. No.	SOA_1	SOA_2	Avg. SOA_1 mass concentration / µg m^{-3}	Avg. SOA_2 mass concentration / µg m^{-3}	Avg. mass concentration when both SOA types are present / µg m^{-3}	Collection time and method
1	α-pinene/O_3	β-caryophyllene/O_3	34 ± 0.35*	43 ± 7.4	89 ± 7.9	22–26 h MOSSI
3	α-pinene/O_3	Catechol/O_3	41 ± 14.3	41 ± 14.5	91 ± 22.9	22–26 h MOSSI
4	Catechol/O_3	β-caryophyllene/O_3	42 ± 12.8	39 ± 12.1	93 ± 5.0	22–26 h MOSSI

* sampling time for pure α-pinene SOA was ~10 min

S3 Effect of particle generation and collection method on phase behavior

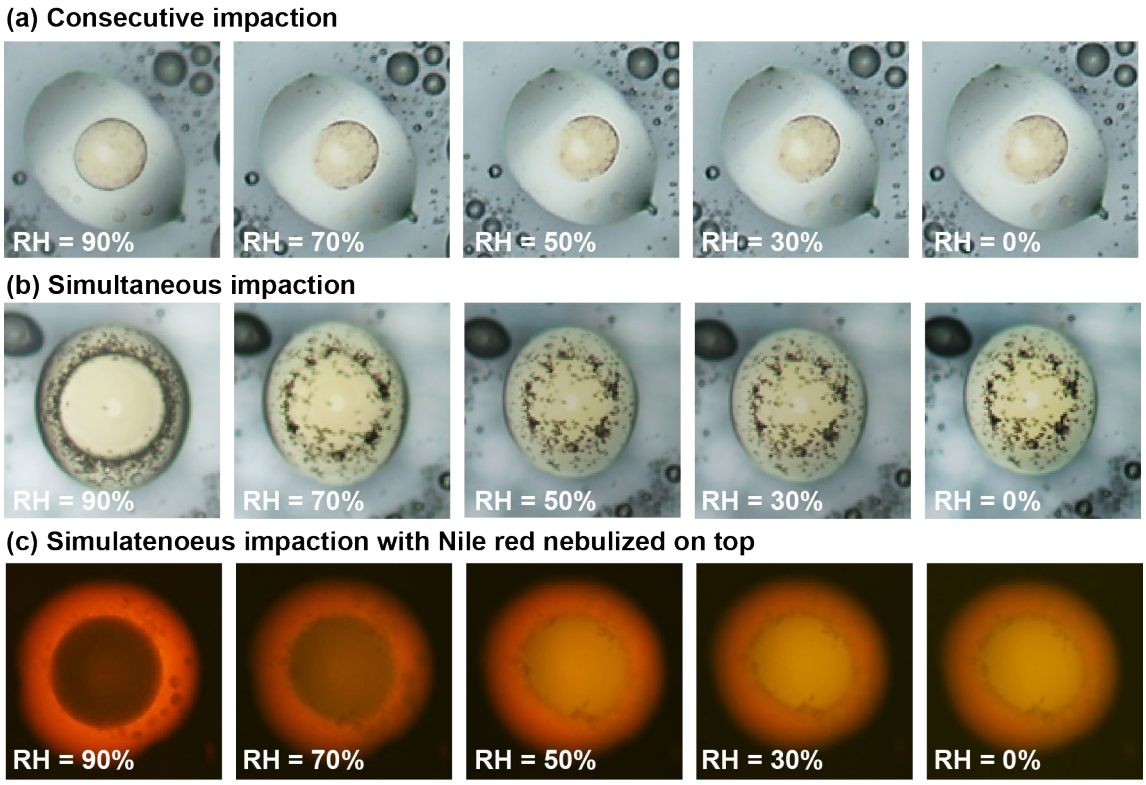

Figure S2: Example of effect of collection method on phase behavior of internal SOA+SOA mixtures for particles containing β-caryophyllene SOA material (O/C = 0.40) and catechol SOA material (O/C = 0.88). (a) Optical microscope images of β-caryophyllene SOA material deposited onto glass slide containing previously deposited catechol SOA material. (b) Optical microscope images of simultaneously impacted β-caryophyllene SOA material and catechol SOA material from the UBC environmental chamber. (c) Fluorescence microscope images of the same sample as in panel (b), but with trace amounts of Nile red nebulized on top of SOA+SOA particles.

S4 Estimation of SOA-to-SOA mixing ratio in internally mixed SOA+SOA particles

The ratio of the amount of the different SOA types within internally mixed SOA+SOA particles can impact the phase behavior. Here, we have used two different approaches to estimate the ratio of the SOA types for mixtures prepared by the consecutive generation and impaction method and the simultaneous generation and impaction method, as detailed below.

S4.1 Estimation of SOA-to-SOA mixing ratio for consecutive generation and impaction method experiments

In order to estimate the ratio of the different SOA types within individual particles, we assumed that the ratio of the volumes of the different phases equals the ratio of the different SOA types. Hence, this approach is only applicable for phase-separated particles but cannot be applied to single-phase SOA+SOA particles, and further neglects partial miscibility between the two SOA types within a mixture. A caveat associated with this approach stems from assuming absence of yield enhancements between the two SOA types and associated impacts on the mixing ratio. In other words, the yield enhancement of SOA_1 caused by SOA_2 is assumed to be similar to the yield enhancement of SOA_2 by SOA_1. This assumption, although idealized, allowed us to estimate the SOA-to-SOA mixing ratio from the spatial arrangement of the different SOA phases within internally mixed particles. Here, we used a laser scanning confocal microscope (Zeiss, model: Axio Observer 510 MP) to measure the three-dimensional arrangement within individual phase-separated SOA+SOA particles. Confocal microscopy enables recording of two-dimensional images of the deposited SOA+SOA particles at different focal depths of the particles. By changing the focal depth, i.e., scanning the focal plane along the height (z-dimension) of the particles, a series of two-dimensional images results, that can be combined into so-called z-stacks. From these z-stacks the structure of the SOA+SOA particles, i.e., the spatial arrangement of the two SOA phases, could be reconstructed for individual particles. For mixtures that resulted in single phase SOA+SOA particles, the SOA-to-SOA mixing ratio could not be estimated using confocal microscopy. Nonetheless, given that the same method was used for generating internally mixed SOA+SOA particles, we assume that the mixing ratios are likely comparable to the values observed for the phase-separated SOA+SOA particles.

For the mixtures produced by the consecutive generation and impaction method and that resulted in phase-separated SOA+SOA particles, two main morphologies were observed: i) particles where the outer SOA phase formed a spherical cap, hereafter referred to as spherical calotte, and the inner SOA phase formed a sphere within the spherical calotte, ii) particles where the outer SOA phase formed a spherical calotte and the inner SOA phase formed a cylinder within the spherical calotte.

Example confocal microscope images for each of the two morphologies are shown in Fig. S3, along with schematics illustrating the morphologies.

Independent of the morphology of the SOA+SOA particles, the volume of the entire particle was estimated by assuming a spherical cap-shaped particle, where the volume can be calculated following, e.g., Iwamatsu (2018) as:

$$V_{SOA+SOA} = \frac{4}{3}\pi R\varphi(\theta_{SOAout,s}), \quad \text{(S1)}$$

with,

$$\varphi(\theta_{SOAout,s}) = \frac{(2+cos\theta_{SOAout,s})(1-cos\theta_{SOAout,s})^2}{4}, \quad \text{(S2)}$$

where $\theta_{SOAout,s}$ is the contact angle between the outer SOA phase and the hydrophobic glass slide (schematic in Fig. S3c and d), that was determined from our confocal microscopy images following established methods (Chesna et al., 2016). Furthermore, R denotes the radius of the spherical cap-shaped SOA particle on the flat glass substrate. The radius of the spherical cap, R, is related to the radius of the cross-sectional area of the spherical cap with the glass substrate, r_{SOAout}, (the radius of the circle when looking at the particle from above, i.e., in the top-down view) by $R = r_{SOAout}/\sin\theta_{SOAout,s}$ (schematic in Fig. S3a).

While the volume of the entire SOA+SOA particle was always estimated by assuming a spherical-cap morphology for all our particles, the method to estimate the volume of the inner SOA phase differed depending on the morphology observed in the confocal microscopy images, as illustrated by our schematics shown in Fig. S3.

For cases where the inner SOA phase formed a sphere within the spherical calotte (Fig. S3a), the volume of the inner SOA phase was simply calculated as the volume of a sphere. In cases where multiple spheres were present within the spherical calotte, the volume of the inner SOA phase was calculated as the sum of the volumes of the multiple spheres.

For cases where the inner SOA phase formed a cylinder (Fig. S3b), extending from the glass substrate all the way to the surface of the SOA+SOA particle, the volume of the inner SOA phase was approximated by the volume of a cylinder:

$$V_{SOAin} = \pi r_{SOAin}^2 \cdot h_{SOAin}. \quad \text{(S3)}$$

Here h_{SOAin} is the height of the cylinder formed by the inner SOA phase, marking the largest vertical extent between the hydrophobic glass slides and the interface formed by the inner SOA phase and the air (Fig. S3b). We point out that the contact angle between the inner SOA phase and the hydrophobic glass slides was often a few degrees larger than 90 ° (vertical cross sections in Fig. S3b). In these cases, the "tube-like" volume of a perfect cylinder slightly underestimates the volume of the inner SOA phase, by not capturing the bulges along the height of the cylinder contributing to the volume of the inner SOA phase. At the same time, the volume of a perfect cylinder slightly overestimates the volume of the inner phase, by not accounting for the curvature of the interface formed by the inner SOA phase and the air. In our SOA+SOA particles these effects roughly cancel out, making the assumption of a cylindrical inner SOA phase a reasonably first order approximation. With the volume of the entire SOA+SOA particle and the volume of inner SOA phase calculated, the volume of the outer SOA phase was simply approximated as the difference in these two volumes, ultimately allowing us to estimate the (volume) ratio of the two SOA phases.

For each mixture generated using the consecutive generation and impaction method, which showed phase-separated particles, a new hydrophobic glass slide with SOA+SOA particles was prepared in an identical manner as for the phase behavior analysis and confocal microscopy images were taken to estimate the SOA-to-SOA ratios. Eight individual SOA+SOA particles were analyzed for each mixture that resulted in phase-separated particles. A summary of the estimated SOA-to-SOA ratios following this approach is given in Table S5. The type of SOA material making up the outer and inner phase was identified by exposing the phase-separated SOA+SOA particles to RH values between ~90% to ~101% and observing the growth of the individual phases resulting from uptake of water. The phase with the larger change in size was attributed to the SOA type with the larger O/C ratio, consistent with a higher hygroscopicity, which for the phase-separated SOA+SOA mixtures tested was always the inner phase.

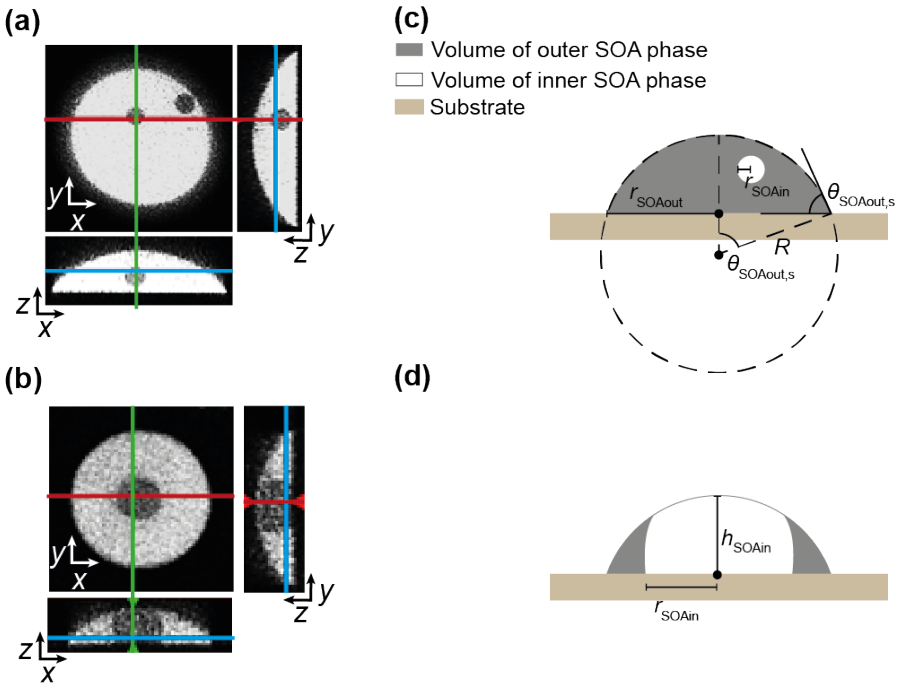

Figure S3: Example confocal microscopy images (a, b) and schematics illustrating the corresponding three-dimensional arrangements (c, d) of the two SOA phases within the deposited SOA+SOA particles for the two dominant arrangements observed in our experiments: (a, c) The inner SOA phase forming spheres within the outer phase having the shape of a spherical calotte and (b, d) the inner SOA phase forming a cylinder within the spherical calotte-shaped outer phase. In each confocal microscopy image, the coordinates are indicated by the arrows. Large top-down views show particles in the x-y plane. The smaller images at the bottom and right denote cross-sections along the green (x-z plane) and red (y-z plane) lines. The blue lines within the vertical cross sections indicate the focal plane corresponding to the x-y plane of the top-down image depicted.

Table S5: Overview of experiments where the consecutive generation and impaction method was used for the generation of SOA+SOA particles and phase separated particles were observed between relative humidities of 90% to 0%. Tabulated are the experiment number and the average (minimum/maximum) SOA-to-SOA (volume) mixing ratios estimated from the confocal microscopy analysis, given as V_{SOAin}/V_{SOAout}, where the inner phase corresponds to the SOA phase with the higher O/C ratio. Also indicated in parenthesis are the number of individual two-phase SOA+SOA particles corresponding to each of the two morphology types based on the confocal microscopy analysis (Fig. S3).

Exp. No.	SOA_1	SOA_2	Avg. (min/max) V_{SOAin}/V_{SOAout} volume ratio	Number of particles with morphology as in Fig. S3a	Number of particles with morphology as in Fig. S3b
6	β-caryophyllene/O_3	Toluene/OH	0.231 (0.012/0.68)	3	5
9	Farnesene/O_3	Catechol/O_3	0.563 (0.201/0.954)	0	8
10	Farnesene/O_3	Toluene/OH	0.581 (0.181/0.867)	0	8
14	Valencene/O_3	Catechol/O_3	0.065 (0.001/0.4)	6	2
15	Valencene/O_3	Toluene/OH	0.492 (0.001/0.806)	3	5

S4.2 Estimation of SOA-to-SOA mixing ratio for simultaneous generation and impaction method experiments

For the mixtures generated using the simultaneous generation and impaction method, another approach was used to estimate the individual contribution of each SOA type within internally mixed SOA+SOA particles. As described in Section S2.2, the particle mass loadings of each SOA type were sampled individually at the beginning and end of each experiment when only one of the SOA types was present within the UBC-EC (Fig. S1). The SOA-to-SOA mass mixing ratio was then simply estimated from the ratio of the average organic mass concentrations when only either one of the SOA types was present within the UBC-EC. The resulting SOA-to-SOA mixing ratios along with the average organic mass concentrations of the individual SOA types before and after each mixing experiment are summarized in Table S6. Also tabulated for comparison are the total organic mass concentrations measured when both SOA types were present within the environmental chamber. Using the OPC mass loadings to estimate the SOA-to-SOA mixing ratios has the advantage that mixing ratios can also be estimated for mixtures

that resulted in single-phase particles. At the same time, this approach neglects possible SOA mass enhancement and associated changes in mixing ratio. Therefore, we acknowledge that the mixing ratios estimated here represent first-order approximations of the true SOA-to-SOA mixing ratios.

Table S6: Overview of experiments where the simultaneous generation and impaction method was used for the generation of SOA+SOA particles. Tabulated are the experiment number and the different SOA types, along with the average organic particle mass loadings for periods when only one SOA type was present within the chamber and for periods when two SOA types were simultaneously present within the chamber. Also listed is the SOA-to-SOA volume mixing ratio estimated as the ratio of the average OPC-based mass loadings before and after an experiment when only SOA_1 or only SOA_2 were present within the chamber and assuming the same density for both SOA types. The values in parenthesis indicate the standard error of the mass loading, given as two standard deviations.

Exp. No.	SOA_1	SOA_2	Avg SOA_1 mass concentration / µg m^{-3}	Avg SOA_2 mass concentration / µg m^{-3}	Avg. total organic aerosol mass when both SOA types are present within EC-UBC / µg m^{-3}	Avg. based estimated SOA_1-to-SOA_2 volume mixing ratio
1	α-pinene/O_3	β-caryophyllene/O_3	34 ± 0.35*	43 ± 7.4	89 ± 7.9	0.79
3	α-pinene/O_3	Catechol/O_3	41 ± 14.3	41 ± 14.5	91 ± 22.9	1
4	Catechol/O_3	β-caryophyllene/O_3	42 ± 12.8	39 ± 12.1	93 ± 5.0	1.08

* sampling time for pure α-pinene SOA was ~10 min

S5 Experimental setup used to determine elemental ratios for SOA from wash off solutions

Chemical characterization of the different SOA types was performed by AMS measurements. For the SOA types generated in the UBC-EC and UBC-OFR, the aerosol particles were directly sampled in-situ from the respective environmental reactor with the AMS. To characterize the toluene SOA material generated in the HU-OFR using the same AMS instrument, toluene SOA material was first collected onto substrates and shipped to the University of British Columbia (UBC). At UBC, the toluene SOA material was extracted into an aqueous solution, and then the SOA material was re-aerosolized from the aqueous solution and sampled by an AMS. This method was validated using SOA generated from catechol ozonolysis within the UBC-EC.

To this end, SOA material was first collected onto glass slides from a given environmental reactor as described in Section S2. For typical collection times of ~24 h and our experimental conditions, this resulted in approximately 1 mg of a given SOA type impacted onto an individual 12 mm diameter glass slide. To extract the SOA material, a glass slides was then placed into a sterile, conical-bottom centrifuge tube (Cole-Parmer, UNP10404-CP), and 3 ml of high-performance liquid chromatography water (HPLC; Millipore Sigma, HPLC water Plus, ≤ 0.0003% non-volatile impurities, ≤ 7 ppb total organic carbon) were added to each tube. The tubes were then placed onto a shaker (New Brunswick Scientific, C2 Platform Shaker Classic Series) operated at 200 rpm for 60 min. The extracts were then used without further filtration and aerosolized using an atomizer setup. Specifically, the aqueous solutions were nebulized using a TROPOS-atomizer, fed through a custom-built diffusion drier containing molecular sieve (Millipore Sigma, sodium and aluminosilicate, A-type crystal structure, 4 Å pore diameter), and then passed into a ~20 L glass mixing volume. The atomizer was operated at a total flow rate of 3.0 L min^{-1}, using nitrogen (Linde, 5.0 grade) as a carrier gas. The total flow rate into the atomizer is given by the sum of the orifice and the dilution flow rates, whose ratio was manually adjusted using a needle valve to achieve typical dripping rates of ~1 Hz. The aerosols were directly sampled by the AMS from the mixing volume and AMS data was analyzed in an identical fashion as described in the main text. To correct for gas-phase interference, samples were also collected by the AMS for a period of 5-10 min with a particle filter (Whatman, 1851-047, grade QM-A) located before the AMS. The excess flow of the mixing volume was filtered (Pall Inc., HEPA filter) and exhausted into the laboratory. The RH of the exhaust was measured in-situ using a humidity sensor (Vaisala, HMT120/130) and was around 5% for our experimental conditions. In between different wash off experiments using the same SOA type, the atomizer was rinsed by running it with pure Milli-Q water (18.2 MΩ.cm) for ~10 min, and the mixing volume was purged with filtered (Pall Inc., HEPA filter) compressed air, using a flow rate of ~10 L min^{-1}, until the particle counts on the CPC were zero. In between different wash off experiments using different SOA types, the atomizer and mixing volume were completely washed with acetone and ethyl acetate, followed by Milli-Q water.

In Table S7 we list the average O/C ratios determined for the different SOA samples using the wash off approach, as described above. Also tabulated -where available- is the average O/C ratio obtained when sampling the SOA particles in-situ from the environmental reactor. For catechol SOA, we found good comparability for the O/C ratios determined in-situ and for the washed-off samples. Thus, the average O/C ratios from both sampling methods were within experimental uncertainty. We point out that the catechol in-situ samples used for this comparison were probed throughout the same period when the SOA material for the corresponding wash-off experiments was collected, to ensure that the same aerosol population was probed with either approach. Based on the good agreement of the O/C ratios determined for the in-situ and the wash-off catechol SOA experiments, we expect our wash-off method to provide reasonable O/C ratios for highly oxidized SOA material that has similar or larger O/C ratios to the catechol ozonolysis SOA tested here, i.e., SOA material that is expected to be largely water soluble. Applying this method to SOA material generated from toluene photooxidation within the OFR-HU, we find an average O/C ratio of 1.05 ± 0.13. Here, we used this O/C ratio for analysis of the phase behavior of SOA+SOA mixtures containing toluene SOA.

To further test the validity of our wash-off experiments we used a scanning particle mobility analyzer, consisting of a differential mobility analyzer (DMA, TSI Inc., Classifier model 3080, with 3081 column and Krypton radiation source) and a condensation particle counter (CPC, TSI Inc., model 3776 operated in low flow mode), operated at an aerosol-to-sheath flow ratio of 1/10, to continuously sample particles from the mixing volume throughout a wash off experiment. In Fig. S4 we show the volume size distributions corresponding to the samples tabulated in Table S7. The overlapping volume distributions for a given SOA type reveal good reproducibility of our wash off experiments. Also shown in Fig. S4 is the distribution obtained when atomizing pure HPLC water, as a reference blank. The volume distribution of the pure HPLC water shows no clear mode, but only a few counts around diameters around 300 nm in diameter. This is expected, given the high purity of the water used as solvent. By contrast the volume distributions of the SOA wash offs show clear mode diameters between approximately 110 nm to 170 nm. This verifies that the signal results from the dissolved organic material rather than from impurities in the solution.

Table S7. Comparison of O/C ratio of SOA samples, when using the AMS to directly sample the aerosol particles in-situ from the environmental reactor and when sampling aerosol particles collected from the environmental reactor that have been re-aerosolized from an aqueous solution (wash off), as described in the text. All O/C ratios were determined based in V-mode AMS data and applying the improved ambient method(Canagaratna et al., 2015; Aiken et al., 2008). Tabulated are the average O/C ratios for each sample along with the uncertainty (12% relative error), associated with the improved ambient method applied to a multi-species organic mixture (≥ 25 species)(Canagaratna et al., 2015). Also indicated in parenthesis is the range over which the average O/C ratios varied throughout the sampling period. N/A denotes values that are not available.

SOA sample	O/C ratio when sampling in-situ	O/C ratio when sampling wash-off
Catechol/O3 (20220326_162300_EC; collected on siliconized glass slide)	0.98 ± 0.12 (0.97 to 1.0)	0.97 ± 0.12 (0.94 to 1.01)
Catechol/O3 (20220327_152600_EC; collected on siliconized glass slide)	0.95 ± 0.11 (0.93 to 0.97)	1.0 ± 0.12 (0.97 to 1.03)
Catechol/O3 (20220403_141000_EC; collected on siliconized glass slide)	0.94 ± 0.11 (0.93 to 0.96)	0.90 ± 0.11 (0.88 to 0.94)
Catechol/O3 (20220404_125600_EC; collected on siliconized glass slide)	0.94 ± 0.11 (0.92 to 0.96)	0.92 ± 0.11 (0.85 to 0.95)
Toluene/OH (Sample #1, 2021_OFR-HU; collected on fluorinated glass slide)	N/A	1.04 ± 0.12 (1.01 to 1.06)
Toluene/OH (Sample #2, 2021_OFR-HU; collected on fluorinated glass slide)	N/A	1.07 ± 0.13 (1.06 to 1.08)
Toluene/OH (Sample #10, 20220305_OFR-HU; collected on siliconized glass slide)	N/A	1.05 ± 0.13 (0.95 to 1.29)
Toluene/OH (Sample #7, 20220222_OFR-HU; collected on siliconized glass slide)	N/A	1.07 ± 0.13 (0.95 to 1.14)

Toluene/OH (Sample #2, 20220217_OFR-HU; collected on siliconized glass slide)	N/A	1.00 ± 0.12 (0.73 to 1.09)

372

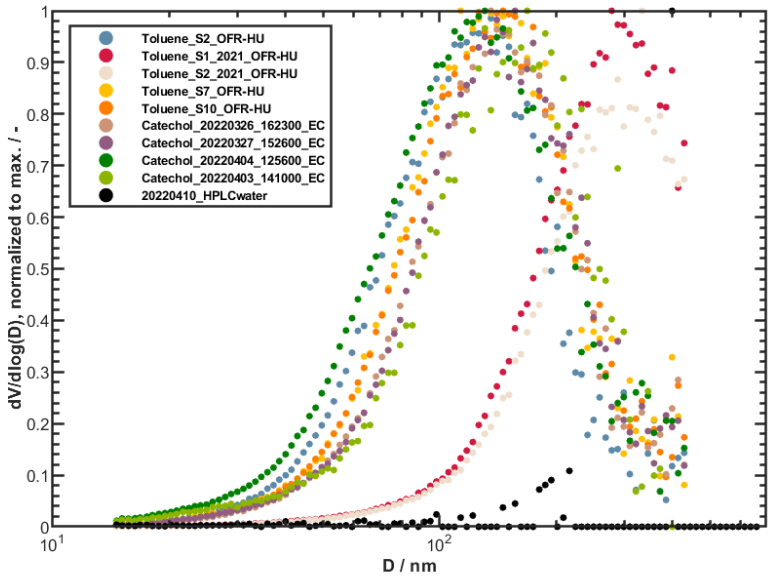

373

374 **Figure S4:** Volume size distributions of the re-aerosolized SOA wash off solutions, as measured by a scanning particle mobility
375 analyzer by sampling from the mixing volume. See text for details.

376

S6 Phase behavior of pure SOA materials

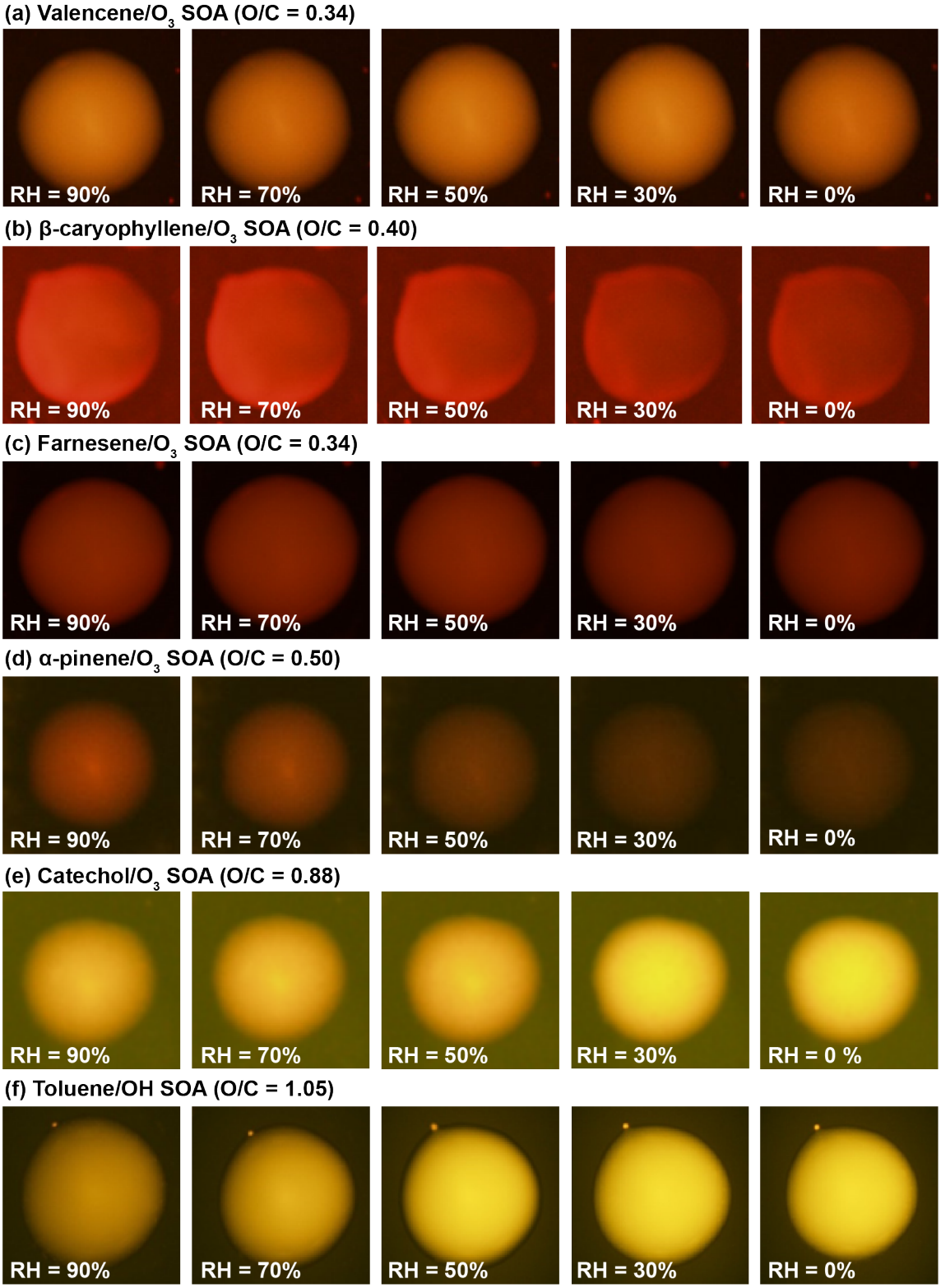

Figure S5: Fluorescence microscopy images of the individual, unmixed secondary organic aerosol (SOA) materials. The SOA type is indicated on top of each row along with its average elemental oxygen-to-carbon (O/C) ratio. The different panels correspond to different relative humidity (RH) values as indicated. The fluorescence color is due to trace amounts of Nile red embedded within the SOA particles.

S7 Phase behavior of internal SOA+SOA mixtures

Shown in the following are the fluorescence microscopy experiments for all the SOA+SOA mixtures studied here. The organization of Fig. S6 to Fig. S10 follows that of the mixing matrix shown in Fig. 2a of the main text, with each Figs. S6–S10 corresponding to one column of Fig. 2a.

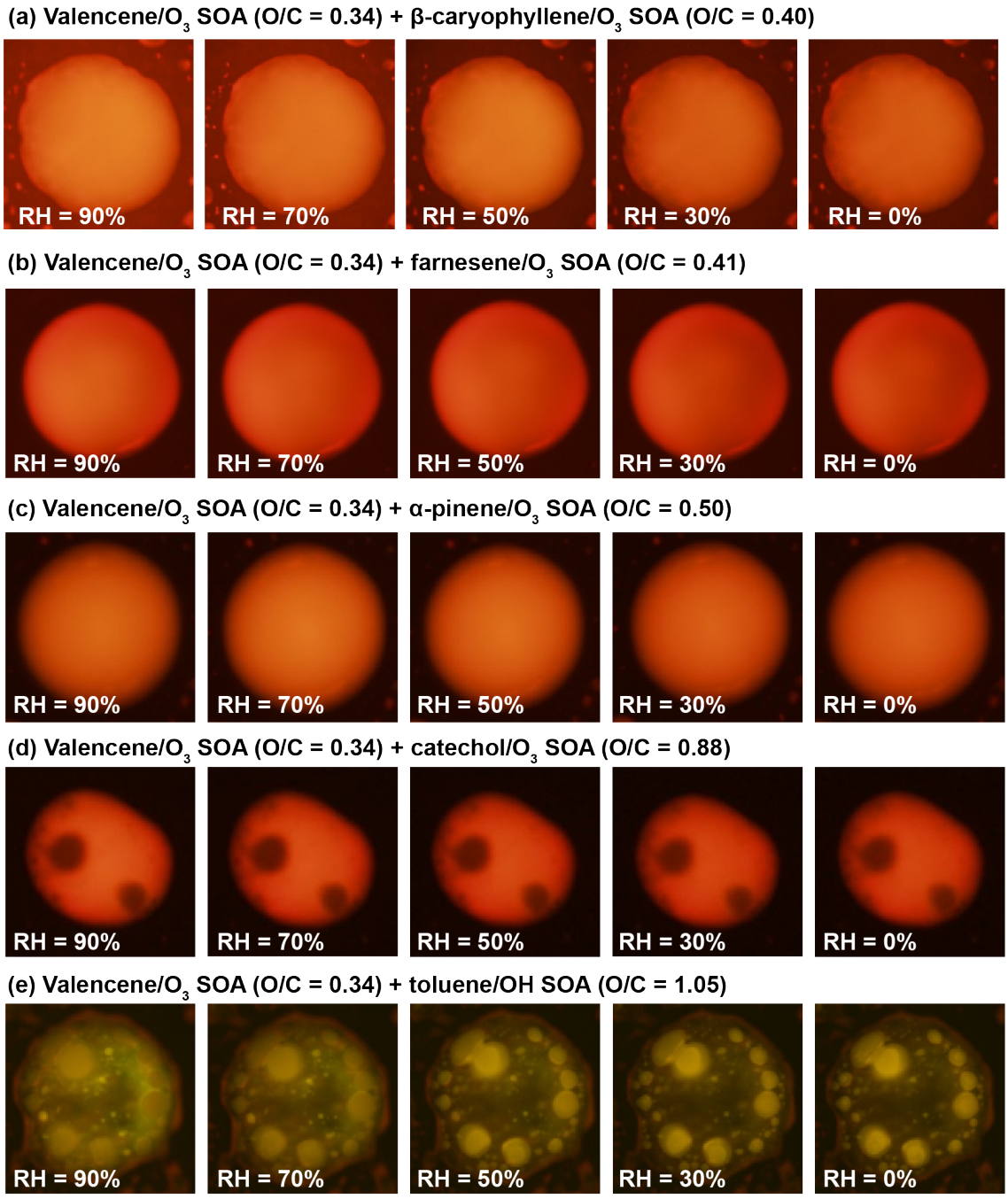

Figure S6: Fluorescence microscopy images of mixtures of secondary organic aerosol (SOA) material derived from valencene ozonolysis with other SOA types. The components of each mixture are given above each row together with the average elemental oxygen-to-carbon (O/C) ratio of the SOA type. The different panels correspond to different relative humidity (RH) values as indicated. The fluorescence color is due to trace amounts of Nile red embedded within the SOA+SOA particles.

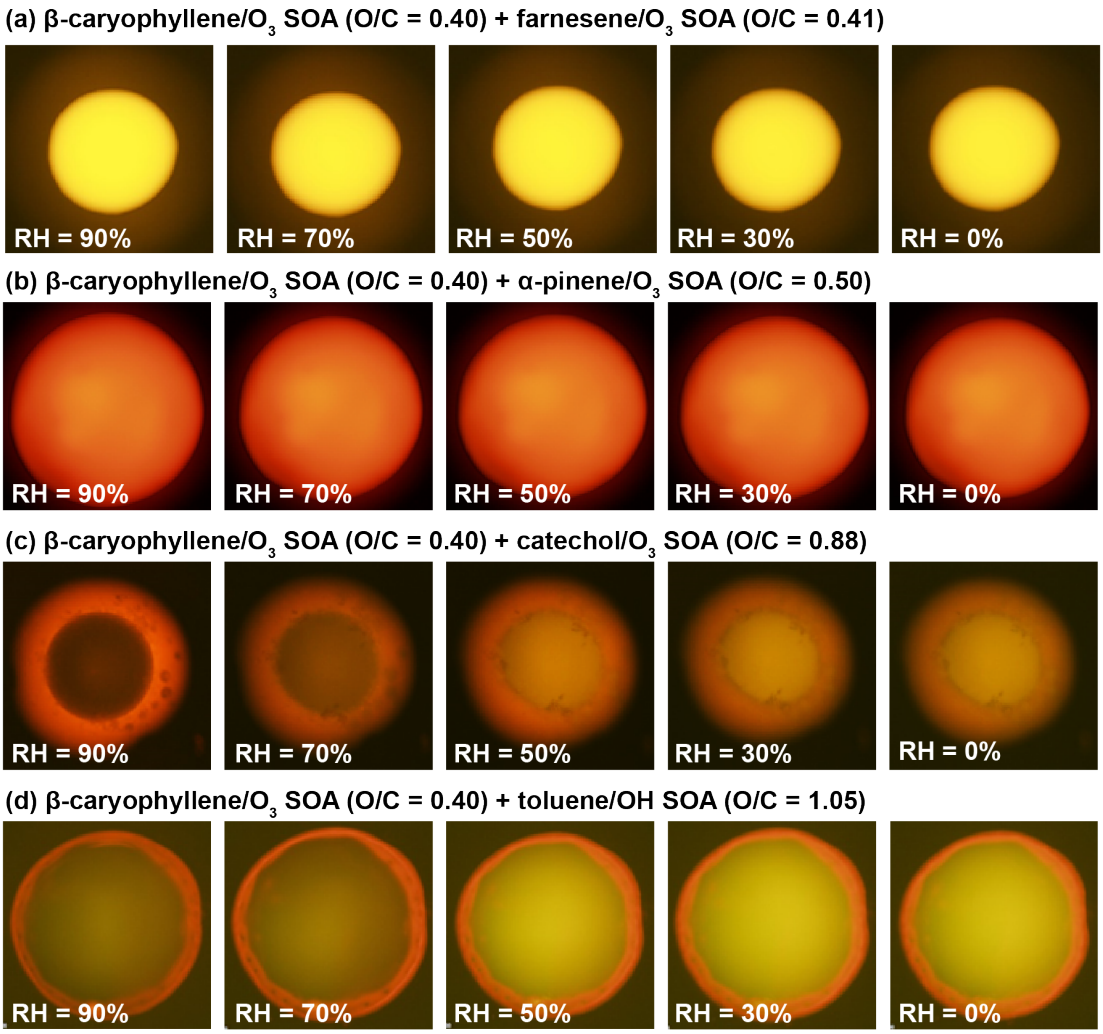

Figure S7: Fluorescence microscopy images of mixtures of secondary organic aerosol (SOA) material derived from β-caryophyllene ozonolysis with other SOA types. The components of each mixture are given above each row together with the average elemental oxygen-to-carbon (O/C) ratio of the SOA type. The different panels correspond to different relative humidity (RH) values as indicated. The fluorescence color is due to trace amounts of Nile red embedded within the SOA+SOA particles.

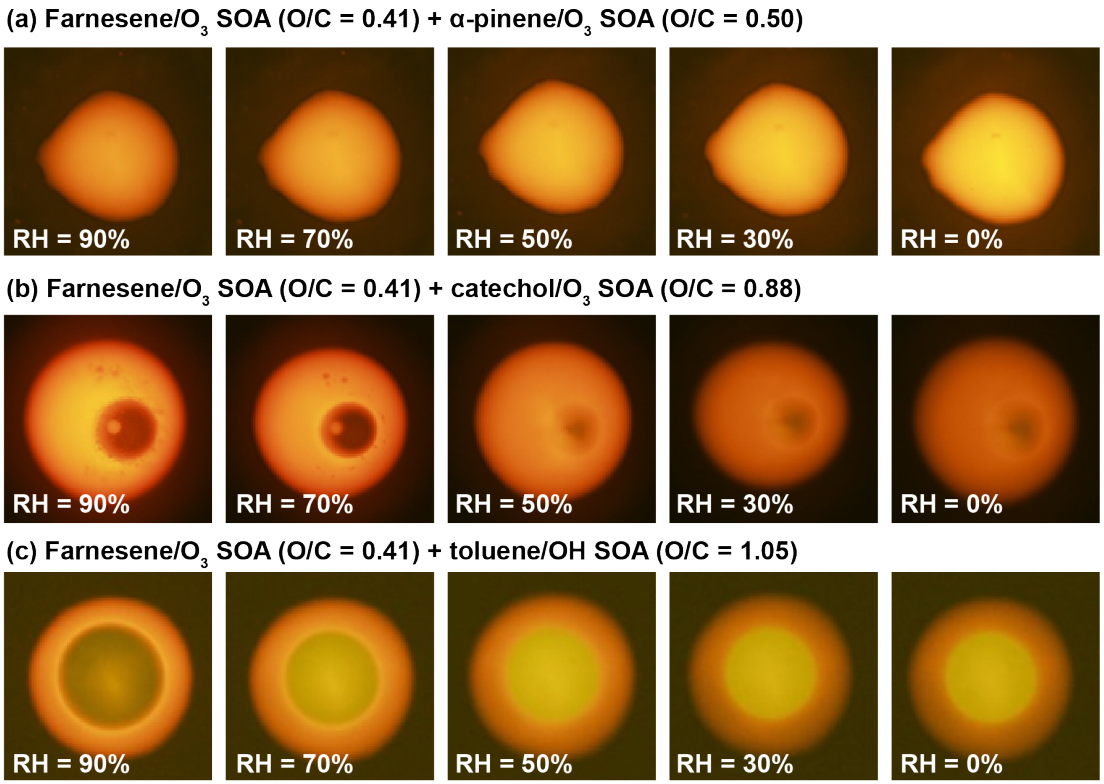

Figure S8: Fluorescence microscopy images of mixtures of secondary organic aerosol (SOA) material derived from farnesene ozonolysis with other SOA types. The components of each mixture are given above each row together with the average elemental oxygen-to-carbon (O/C) ratio of the SOA type. The different panels correspond to different relative humidity (RH) values as indicated. The fluorescence color is due to trace amounts of Nile red embedded within the SOA+SOA particles.

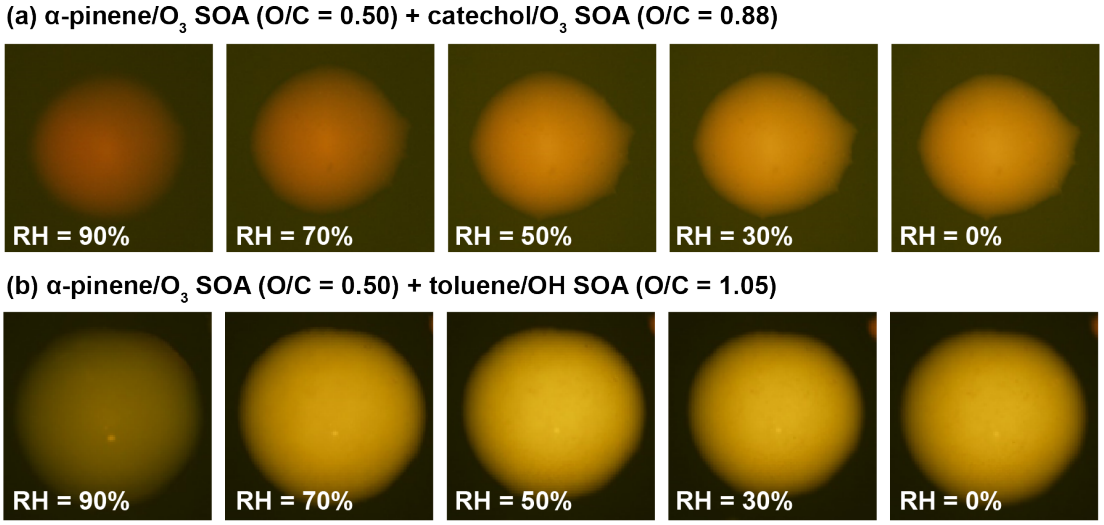

Figure S9: Fluorescence microscopy images of mixtures of secondary organic aerosol (SOA) material derived from α-pinene ozonolysis with other SOA types. The components of each mixture are given above each row together with the average elemental oxygen-to-carbon (O/C) ratio of the SOA type. The different panels correspond to different relative humidity (RH) values as indicated. The fluorescence color is due to trace amounts of Nile red embedded within the SOA+SOA particles.

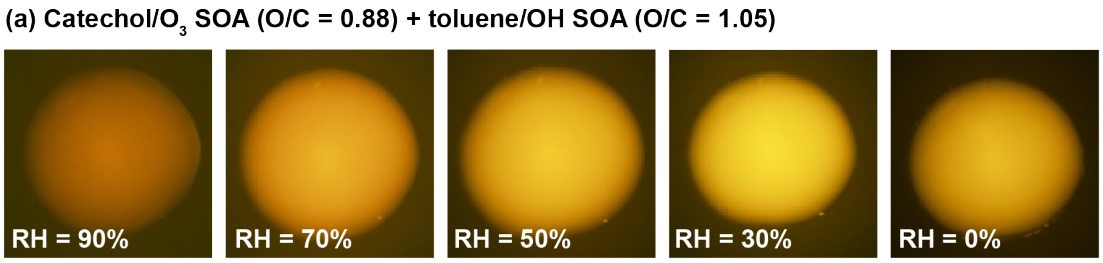

Figure S10: Fluorescence microscopy images of mixtures of secondary organic aerosol (SOA) material derived from catechol ozonolysis with SOA material derived from toluene photooxidation. Also indicated are the average elemental oxygen-to-carbon (O/C) ratio of the SOA types. The different panels correspond to different relative humidity (RH) values as indicated. The fluorescence color is due to trace amounts of Nile red embedded within the SOA+SOA particles.

S8 Phase behavior in SOA particles generated from oxidation of precursor gases emitted from real pine trees

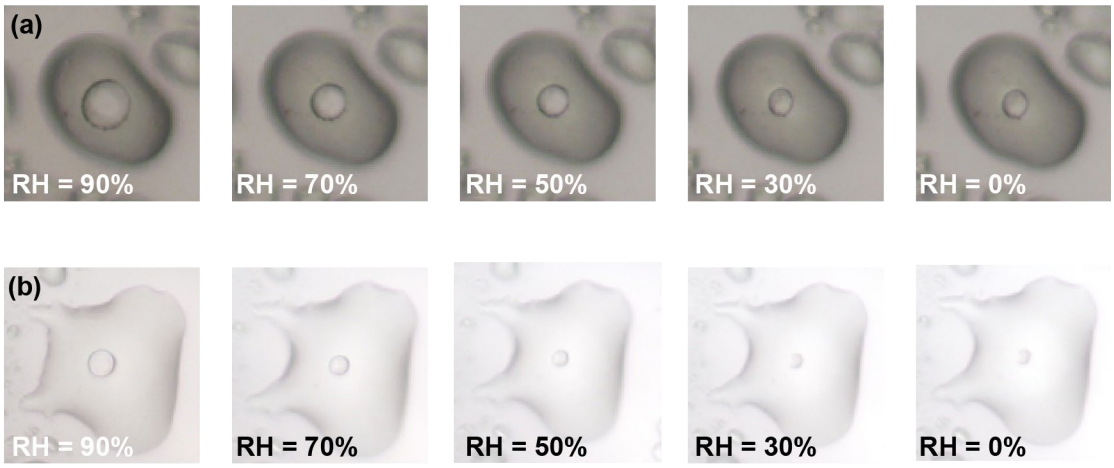

Figure S11: Optical microscope images at different relative humidity (RH) values of SOA material derived from photooxidation of gases emitted from real trees, as described in Smith et al. (in prep.). The images shown in panel (a) and (b) correspond to samples TB2_20210725 and TA3_20210706, respectively, as described by Smith et al. (in prep.).

S9 Phase behavior of SOA+SOA using descriptors beyond Δ(O/C)

While the description of the SOA+SOA phase behavior in terms of the Δ(O/C) value captures the number of phases for most of the mixtures studied here, the inclusion of other parameters in addition to the Δ(O/C) value could further improve the accuracy of such predictions. For example, the evolution of organic aerosol particles along atmospheric aging trajectories is often described by Van Krevelen diagrams, where the aerosol is described in terms of the O/C ratio and the elemental hydrogen-to-carbon (H/C) ratio (e.g. Heald et al., 2010). Using information on the H/C ratio of the SOA types studied here, determined by our AMS measurements (Table S3), and describing the number of phase in terms of both the Δ(O/C) and the Δ(H/C), however, did not lead to a much clearer separation of SOA+SOA mixtures that formed one- and two-phase particles (Fig. S12). Nonetheless, other parameters such as the Hansen solubility parameter that include more chemical information than O/C and H/C ratios (Hansen, 2007) could improve the predictability of the number of phases (Ye et al., 2018a, c). At the same time, the Hansen solubility parameter cannot easily be determined for ambient samples, comes at the cost of adding complexity to the predictive framework, and, as such, is beyond the scope of this study. Another option is to use a more complex thermodynamic model, such as the Aerosol Inorganic–Organic Mixtures Functional Groups Activity Coefficients (AIOMFAC) thermodynamic model together with its phase separation extension (Zuend et al., 2008, 2010; Zuend and Seinfeld, 2013). Such a model could predict the number of phases as well as partially solubility of the components. However, similar to the Hansen solubility parameter, it cannot easily be determined for ambient samples.

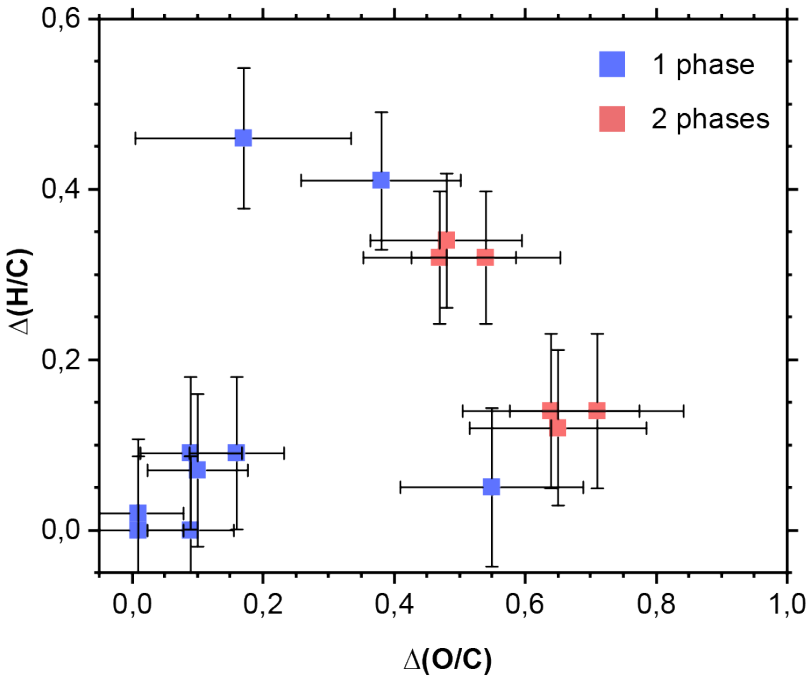

Figure S12: Summary of the number of phases observed in our internally mixed SOA+SOA particles as a function of the absolute difference in the average O/C ratios between the two SOA types within a mixture, $\Delta(O/C) = |O/C_{SOA1}-O/C_{SOA2}|$ and the absolute difference in the average H/C ratios between the two SOA types within a mixture, $\Delta(H/C) = |H/C_{SOA1}-H/C_{SOA2}|$. The horizontal error bars indicate the propagated error from the 12% relative uncertainty of the O/C ratios determined for each SOA type and the vertical error bars indicate the propagated error from the 4% relative uncertainty of the H/C ratios determined for each SOA type (Table S3).

Reference

Aiken, A. C., Decarlo, P. F., Kroll, J. H., Worsnop, D. R., Huffman, J. A., Docherty, K. S., Ulbrich, I. M., Mohr, C., Kimmel, J. R., Sueper, D., Sun, Y., Zhang, Q., Trimborn, A., Northway, M., Ziemann, P. J., Canagaratna, M. R., Onasch, T. B., Alfarra, M. R., Prevot, A. S. H., Dommen, J., Duplissy, J., Metzger, A., Baltensperger, U., and Jimenez, J. L.: O/C and OM/OC ratios of primary, secondary, and ambient organic aerosols with high-resolution time-of-flight aerosol mass spectrometry, 42, 4478–4485, https://doi.org/10.1021/es703009q, 2008.

Canagaratna, M. R., Jimenez, J. L., Kroll, J. H., Chen, Q., Kessler, S. H., Massoli, P., Hildebrandt Ruiz, L., Fortner, E., Williams, L. R., Wilson, K. R., Surratt, J. D., Donahue, N. M., Jayne, J. T., and Worsnop, D. R.: Elemental ratio measurements of organic compounds using aerosol mass spectrometry: characterization, improved calibration, and implications, 15, 253–272, https://doi.org/10.5194/acp-15-253-2015, 2015.

Chesna, J. W., Wiedmaier, B. F., Wang, J., Samara, A., Leach, R. K., Her, T.-H., and Smith, S. T.: Aerial wetting contact angle measurement using confocal microscopy, Meas. Sci. Technol., 27, 125202, https://doi.org/10.1088/0957-0233/27/12/125202, 2016.

Docherty, K. S. and Ziemann, P. J.: Effects of Stabilized Criegee Intermediate and OH Radical Scavengers on Aerosol Formation from Reactions of β-Pinene with O 3, 37, 877–891, https://doi.org/10.1080/02786820300930, 2003.

Dommen, J., Hellén, H., Saurer, M., Jaeggi, M., Siegwolf, R., Metzger, A., Duplissy, J., Fierz, M., and Baltensperger, U.: Determination of the Aerosol Yield of Isoprene in the Presence of an Organic Seed with Carbon Isotope Analysis, Environ. Sci. Technol., 43, 6697–6702, https://doi.org/10.1021/es9006959, 2009.

Gordon, C. A., Ye, J., and Arthur W.H., C.: Secondary Organic Aerosol Formation Enhanced by Organic Seeds of Similar Polarity at Atmospherically Relative Humidity, https://doi.org/10.17975/sfj-2015-009, 2016.

Gorkowski, K., Donahue, N. M., and Sullivan, R. C.: Emulsified and Liquid–Liquid Phase-Separated States of α-Pinene Secondary Organic Aerosol Determined Using Aerosol Optical Tweezers, Environ. Sci. Technol., 51, 12154–12163, https://doi.org/10.1021/acs.est.7b03250, 2017.

Gorkowski, K., Donahue, N. M., and Sullivan, R. C.: Aerosol Optical Tweezers Constrain the Morphology Evolution of Liquid-Liquid Phase-Separated Atmospheric Particles, Chem, 6, 204–220, https://doi.org/10.1016/j.chempr.2019.10.018, 2020.

Hansen, C. M.: Hansen Solubility Parameters: A User's Handbook, Second Edition, Second Edition., CRC Press, 544 pp., 2007.

Heald, C. L., Kroll, J. H., Jimenez, J. L., Docherty, K. S., DeCarlo, P. F., Aiken, A. C., Chen, Q., Martin, S. T., Farmer, D. K., and Artaxo, P.: A simplified description of the evolution of organic aerosol composition in the atmosphere, 37, https://doi.org/10.1029/2010GL042737, 2010.

Hildebrandt, L., Henry, K. M., Kroll, J. H., Worsnop, D. R., Pandis, S. N., and Donahue, N. M.: Evaluating the Mixing of Organic Aerosol Components Using High-Resolution Aerosol

Mass Spectrometry, Environ. Sci. Technol., 45, 6329–6335, https://doi.org/10.1021/es200825g, 2011.

Huang, Y., Mahrt, F., Xu, S., Shiraiwa, M., Zuend, A., and Bertram, A. K.: Coexistence of three liquid phases in individual atmospheric aerosol particles, PNAS, 118, https://doi.org/10.1073/pnas.2102512118, 2021.

Iwamatsu, M.: A generalized Young's equation to bridge a gap between the experimentally measured and the theoretically calculated line tensions, 32, 2305–2319, https://doi.org/10.1080/01694243.2018.1476036, 2018.

Keywood, M. D., Kroll, J. H., Varutbangkul, V., Bahreini, R., Flagan, R. C., and Seinfeld, J. H.: Secondary Organic Aerosol Formation from Cyclohexene Ozonolysis: Effect of OH Scavenger and the Role of Radical Chemistry, Environ. Sci. Technol., 38, 3343–3350, https://doi.org/10.1021/es049725j, 2004.

Kim, D., Stevens, P. S., and Hites, R. A.: Rate Constants for the Gas-Phase Reactions of OH and O3 with β-Ocimene, β-Myrcene, and α- and β-Farnesene as a Function of Temperature, J. Phys. Chem. A, 115, 500–506, https://doi.org/10.1021/jp111173s, 2011.

King, S. M., Rosenoern, T., Shilling, J. E., Chen, Q., and Martin, S. T.: Increased cloud activation potential of secondary organic aerosol for atmospheric mass loadings, 9, 2959–2971, https://doi.org/10.5194/acp-9-2959-2009, 2009.

Kroll, J. H., Donahue, N. M., Cee, V. J., Demerjian, K. L., and Anderson, J. G.: Gas-Phase Ozonolysis of Alkenes: Formation of OH from Anti Carbonyl Oxides, J. Am. Chem. Soc., 124, 8518–8519, https://doi.org/10.1021/ja0266060, 2002.

Liu, P. F., Abdelmalki, N., Hung, H.-M., Wang, Y., Brune, W. H., and Martin, S. T.: Ultraviolet and visible complex refractive indices of secondary organic material produced by photooxidation of the aromatic compounds toluene and *m*-xylene, 15, 1435–1446, https://doi.org/10.5194/acp-15-1435-2015, 2015.

Maclean, A. M., Smith, N. R., Li, Y., Huang, Y., Hettiyadura, A. P. S., Crescenzo, G. V., Shiraiwa, M., Laskin, A., Nizkorodov, S. A., and Bertram, A. K.: Humidity-Dependent Viscosity of Secondary Organic Aerosol from Ozonolysis of β-Caryophyllene: Measurements, Predictions, and Implications, ACS Earth Space Chem., 5, 305–318, https://doi.org/10.1021/acsearthspacechem.0c00296, 2021.

Paulson, S. E., Chung, M. Y., and Hasson, A. S.: OH Radical Formation from the Gas-Phase Reaction of Ozone with Terminal Alkenes and the Relationship between Structure and Mechanism, J. Phys. Chem. A, 103, 8125–8138, https://doi.org/10.1021/jp991995e, 1999.

Robinson, E. S., Saleh, R., and Donahue, N. M.: Organic Aerosol Mixing Observed by Single-Particle Mass Spectrometry, J. Phys. Chem. A, 117, 13935–13945, https://doi.org/10.1021/jp405789t, 2013.

Shilling, J. E., Chen, Q., King, S. M., Rosenoern, T., Kroll, J. H., Worsnop, D. R., McKinney, K. A., and Martin, S. T.: Particle mass yield in secondary organic aerosol formed by the dark ozonolysis of α-pinene, 8, 2073–2088, https://doi.org/10.5194/acp-8-2073-2008, 2008.

Smith, N. R., Crescenzo, G. V., Faiola, C. L., Bertram, A. K., and Nizkorodov, S. A.: Effect of insect infestation on viscosity of Canary Island pine tree SOA, in prep.

Song, C., Zaveri, R. A., Shilling, J. E., Alexander, M. L., and Newburn, M.: Effect of Hydrophilic Organic Seed Aerosols on Secondary Organic Aerosol Formation from Ozonolysis of α-Pinene, Environ. Sci. Technol., 45, 7323–7329, https://doi.org/10.1021/es201225c, 2011.

Song, M., Liu, P., Martin, S. T., and Bertram, A. K.: Liquid–liquid phase separation in particles containing secondary organic material free of inorganic salts, 17, 11261–11271, https://doi.org/10.5194/acp-17-11261-2017, 2017.

Ye, J., Gordon, C. A., and Chan, A. W. H.: Enhancement in Secondary Organic Aerosol Formation in the Presence of Preexisting Organic Particle, Environ. Sci. Technol., 50, 3572–3579, https://doi.org/10.1021/acs.est.5b05512, 2016a.

Ye, J., Van Rooy, P., Adam, C. H., Jeong, C.-H., Urch, B., Cocker, D. R., Evans, G. J., and Chan, A. W. H.: Predicting Secondary Organic Aerosol Enhancement in the Presence of Atmospherically Relevant Organic Particles, ACS Earth Space Chem., 2, 1035–1046, https://doi.org/10.1021/acsearthspacechem.8b00093, 2018a.

Ye, Q., Robinson, E. S., Ding, X., Ye, P. L., Sullivan, R. C., and Donahue, N. M.: Mixing of secondary organic aerosols versus relative humidity, 113, 12649–12654, https://doi.org/10.1073/pnas.1604536113, 2016b.

Ye, Q., Upshur, M. A., Robinson, E. S., Geiger, F. M., Sullivan, R. C., Thomson, R. J., and Donahue, N. M.: Following Particle-Particle Mixing in Atmospheric Secondary Organic Aerosols by Using Isotopically Labeled Terpenes, 4, 318–333, https://doi.org/10.1016/j.chempr.2017.12.008, 2018b.

Ye, Q., Gu, P., Li, H. Z., Robinson, E. S., Lipsky, E., Kaltsonoudis, C., Lee, A. K. Y., Apte, J. S., Robinson, A. L., Sullivan, R. C., Presto, A. A., and Donahue, N. M.: Spatial Variability of Sources and Mixing State of Atmospheric Particles in a Metropolitan Area, Environ. Sci. Technol., 52, 6807–6815, https://doi.org/10.1021/acs.est.8b01011, 2018c.

Yee, L. D., Isaacman-VanWertz, G., Wernis, R. A., Meng, M., Rivera, V., Kreisberg, N. M., Hering, S. V., Bering, M. S., Glasius, M., Upshur, M. A., Gray Bé, A., Thomson, R. J., Geiger, F. M., Offenberg, J. H., Lewandowski, M., Kourtchev, I., Kalberer, M., de Sá, S., Martin, S. T., Alexander, M. L., Palm, B. B., Hu, W., Campuzano-Jost, P., Day, D. A., Jimenez, J. L., Liu, Y., McKinney, K. A., Artaxo, P., Viegas, J., Manzi, A., Oliveira, M. B., de Souza, R., Machado, L. A. T., Longo, K., and Goldstein, A. H.: Observations of sesquiterpenes and their oxidation products in central Amazonia during the wet and dry seasons, 18, 10433–10457, https://doi.org/10.5194/acp-18-10433-2018, 2018.

Zhang, X., Ortega, J., Huang, Y., Shertz, S., Tyndall, G. S., and Orlando, J. J.: A steady-state continuous flow chamber for the study of daytime and nighttime chemistry under atmospherically relevant NO levels, 11, 2537–2551, https://doi.org/10.5194/amt-11-2537-2018, 2018.

Zuend, A. and Seinfeld, J. H.: A practical method for the calculation of liquid–liquid equilibria in multicomponent organic–water–electrolyte systems using physicochemical constraints, Fluid Phase Equilibria, 337, 201–213, https://doi.org/10.1016/j.fluid.2012.09.034, 2013.

565 Zuend, A., Marcolli, C., Luo, B. P., and Peter, T.: A thermodynamic model of mixed organic-
566 inorganic aerosols to predict activity coefficients, 8, 4559–4593, https://doi.org/10.5194/acp-
567 8-4559-2008, 2008.

568 Zuend, A., Marcolli, C., Peter, T., and Seinfeld, J. H.: Computation of liquid-liquid equilibria
569 and phase stabilities: implications for RH-dependent gas/particle partitioning of organic-inor-
570 ganic aerosols, 10, 7795–7820, https://doi.org/10.5194/acp-10-7795-2010, 2010.

571